Aerospace Science and Technology 153 (2024) 109420

Contents lists available at ScienceDirect

Aerospace Science and Technology

journal homepage: www.elsevier.com/locate/aescte

Wind-tunnel experimental investigation on rotor-rotor aerodynamic interaction in compound helicopter configuration

Andrea Colli *, Alex Zanotti, Giuseppe Gibertini

Dipartimento di Scienze e Tecnologie Aerospaziali (DAER), Politecnico di Milano, Via La Masa, 34, Milano, 20156, Italy

ARTICLE INFO

Communicated by George Barakos

Keywords:
Compound helicopter
Wake interaction
Wind tunnel

ABSTRACT

In recent years, the compound helicopter configuration, featuring the addition of lateral propellers to a helicopter main rotor, has gained renewed interest for its ability to achieve higher flight speed. The aerodynamic behaviour of compound rotorcraft is dominated by mutual interactions between the rotors and the wakes they generate, which can affect their performance and the handling qualities of the aircraft. In order to study the effects of the rotor-wake and wake-wake interactions, a test rig was developed and an extensive wind-tunnel test campaign was carried out measuring the performance of rotor and propellers under different flight conditions. Hovering flight and forward flight at different advance ratios were considered, as well as crosswind flight under various wind directions. In general, an increase in thrust for both main rotor and propellers is found due to the interaction. In particular, the significant increase in the propeller thrust is attributed to the influence of the main rotor downwash, which impacts edgewise on the propellers. In some specific conditions, a decrease in the propeller's thrust is observed, which might be related to blade-vortex interaction (BVI) effects. To aid in the interpretation of the experimental results, numerical simulations with a mid-fidelity aerodynamic code were also performed.

1. Introduction

The term "compound helicopter" is usually used to refer to a rotorcraft in which a main rotor is used in conjunction with a secondary propulsion system, wings, or both. The idea behind this configuration is to alleviate the aerodynamic load of the main rotor by providing additional thrust and/or lift forces, therefore removing the limitations to high-speed flight that compressibility effects and retreating blade stall impose on conventional helicopters. Moreover, increased maneuverability, reduced overall vibration levels, and augmented operative range are additional benefits expected from a compound architecture [1].

The concept of a compound helicopter dates back to the 1950s, but, after these early efforts, the research stalled, favouring the tilt-rotor design instead [1,2]. In the last years, the compound architecture has gained new interest [3,4], as its advantages over conventional helicopter, while maintaining the key capability of hovering flight, would be of chief value for numerous scenarios, particularly for search and rescue (SAR) and emergency medical services (EMS), and, in general, for medium-range transportation and any application requiring vertical take-off and landing (VTOL) features.

From an aerodynamic point of view, one of the challenges in designing a compound helicopter is presented by the interaction of the main rotor and its wake with the propellers and their own wakes. As these complex interactions can affect the aerodynamic performance, the level of vibration and the noise production of the aircraft, their investigation is significant for the design phase.

Recent literature on compound helicopters has tackled the issue, both from an experimental and a numerical point of view. High-fidelity simulations of a complete configuration, including a main rotor, twin lateral rotors, and wings have been described in [5–8], for different flight conditions such as hovering, high-speed cruise, and crosswind. The same configuration was analyzed in similar conditions by [9], with a particular focus on the effects of the wings. The works by [10,11] also feature computational fluid dynamics (CFD) simulations of a main rotor and twin propeller configuration in hovering conditions.

In the different flight conditions, the propellers of a compound configuration are fully or partially immersed in the main rotor downwash, which is directed parallel to the propellers' disk. As a result, the propellers are experiencing a very strong relative inflow component directed perpendicular to their axis. The effects of these additional velocity

* Corresponding author.
E-mail addresses: andrea.colli@polimi.it (A. Colli), alex.zanotti@polimi.it (A. Zanotti), giuseppe.gibertini@polimi.it (G. Gibertini).

https://doi.org/10.1016/j.ast.2024.109420
Received 7 June 2024; Received in revised form 16 July 2024; Accepted 22 July 2024
Available online 26 July 2024

Notation

c	chord [m]
CCW	counter-clockwise
CFD	computational fluid dynamics
$C_{Q,MR}$	main rotor torque coefficient, $C_{Q,MR} = \frac{Q_{MR}}{\pi\rho\Omega^2 R^5}$
$C_{Q,RP}$	propeller torque coefficient, $C_{Q,RP} = \frac{Q_{RP}}{\rho n^2 D^5}$
$C_{T,MR}$	main rotor thrust coefficient, $C_{T,MR} = \frac{T_{MR}}{\pi\rho\Omega_{MR}^2 R_{MR}^4}$
$C_{T,RP}$	propeller thrust coefficient, $C_{T,RP} = \frac{T_{RP}}{\rho n^2 D^4}$
EJ	flexural rigidity [N m^2]
EMS	emergency medical services
ESC	electronic speed controller
FM	main rotor figure of merit, $FM = \frac{C_{T,MR}^{3/2}}{\sqrt{2}C_{Q,MR}}$
GJ	torsional rigidity [N m^2 rad^{-1}]
LHD	Leonardo Helicopters
LP	left propeller
LPP	pusher left propeller
m	blade mass per unit length [kg m^{-1}]
$\mathrm{Ma}_{\mathrm{tip}}$	blade tip Mach number
MR	main rotor
n	propeller revolutions per second $n = \frac{\Omega}{2\pi}$ [s^{-1}]
PWM	pulse-width modulation
Q	torque [N m]
Q_{crit}	Q-criterion
R	radius [m]
r	blade span-wise coordinate [m]
RP	right propeller
SAR	search and rescue
T	thrust [N]
U_{ave}	average of velocity magnitude [m s^{-1}]
V_∞	free-stream speed [m s^{-1}]
V_{tip}	blade tip velocity [m s^{-1}]
VTOL	vertical take-off and landing
η_{RP}	propeller efficiency, $\eta_{RP} = \frac{C_{T,RP}}{C_{Q,RP}}$
θ	blade pitch at 75% R [deg]
μ	advance ratio, $\mu = \frac{V_{\mathrm{tip,\,MR}}}{V_\infty}$
ρ	air density [kg m^{-3}]
ϕ	blade azimuth angle [deg]
ψ	angle of free-stream direction [deg]
Ω	rotational speed [rad s^{-1}]

Subscripts

LP	left propeller
MR	main rotor
RP	right propeller

components have been known for a long time, and were already noticed in the pioneering, albeit crude by today's standards, experiments on propellers by [12,13]. A thorough theoretical analysis in terms of induced velocity distribution was initiated by Glauert [14] and continued through the middle of the last century, owing to the interest in tilt-rotor aircraft [15–17]. More recent efforts, testifying to the renewed interest in these topics from various fields of rotary-wing aerodynamics, can be found in [18–20].

As detailed by these investigations, the effect is twofold. Firstly, the blades of the propeller experience a variation in the tangential component of the relative velocity as they rotate, as the external velocity either adds to or subtracts from the velocity due to the blade rotation. This is a well-known phenomenon related to helicopter rotors in forward flight, but when studying its effect on propellers it must be taken into account that no cyclic pitch variation is possible and that no hinges are present, if one neglects the bending of the blades. In general, therefore, there will be a decided asymmetry in the thrust distribution over the propeller's disk, and in-plane forces and out-of-plane rotational moments will arise, which are referred to as "1P loads" [18]. In the case of a compound helicopter configuration, the up-stroking blade of the propeller sees a higher tangential component of the relative velocity, which results in a higher relative incidence and dynamic pressure, while the vice-versa is true for the down-stroking blade. Secondly, the effect of the velocity component perpendicular to the disk is to displace the propeller's wake, therefore altering the distribution of the induced flow on the propeller itself. The resulting inflow distribution is skewed towards the rear of the propeller's disk, i.e. the induced velocity is lower in the region facing the incoming free-stream flow (the upper side, considering the main rotor downwash effect on the propellers), and greater in the opposite region.

In general, these two effects result in an increase in the propeller's generated thrust with respect to the conditions with no velocity component perpendicular to its axis, as confirmed by the available literature. Concerning the present case of the compound helicopter configuration, however, some distinctions have to be made. Firstly, the main rotor downwash is not completely equivalent to a uniform addition free-stream component. Indeed, the velocity distribution in the main rotor wake is not axially uniform, since the blade loading increases over the blade span, resulting in a higher downwash velocity. Moreover, depending on the conditions, the lateral propellers might be only partially immersed in the main rotor's downwash. Secondly, significant vortical structures are present in the rotor's wake, especially the blade-tip vortices, whose effects upon the direct interaction with the below propellers are fundamentally different from the ones mentioned above and are not amenable to simple and sufficiently general theoretical descriptions. To this latter category belong the phenomena known as blade-vortex interactions (BVIs), which, in recent years, was shown to have an important effect on the performances of helicopter rotors, including the triggering of dynamic stall [21–23].

In the last years, the Action Group AG-25 operated in the GARTEUR framework was aimed at investigating specifically rotor-rotor and rotor-wake interactions [24]. Among the activities, [25] investigated experimentally the interaction of a main rotor and a lateral propeller in hovering and advanced flight, and later the same configuration was reproduced numerically by [26]. In general, all the studies agree in reporting a favourable interaction between the main rotor downwash flow and the lateral propellers, which tends to increase the propellers' thrust and efficiency. Correspondingly, a positive effect on the main rotor is observed, although smaller in magnitude. The presence of the wings can also have an important influence on the thrust generated by the propellers, in some cases negating the gain from the main rotor wake.

The present work, which was also part of the aforementioned GARTEUR AG-25 project, presents the results of a wind-tunnel test campaign conducted at Politecnico di Milano and involving a typical compound aircraft configuration, with a main rotor and two propellers, one on each side of the aircraft. A wide variety of conditions was tested, including hovering and forward flight, with particular regard to crosswind flight, at different advance ratios and wind directions, privileging low-speed conditions. For this reason, the propellers were considered mainly to have an anti-torque function. The main objective of the study was to

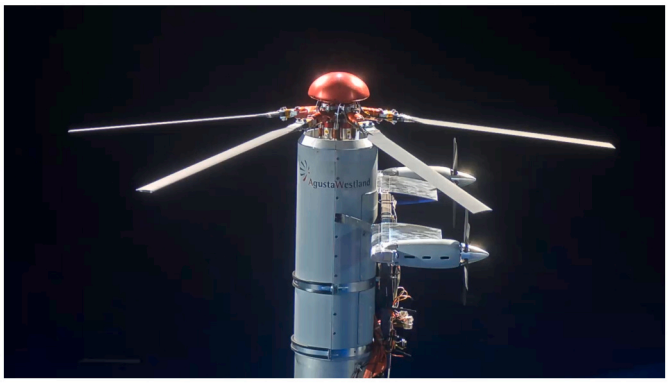

Fig. 1. The upper portion of the complete test rig with the main rotor and both propellers installed. View from the left.

experimentally characterize the mutual interaction between the main rotor and the lateral propellers, in terms of the aerodynamic loads generated, by comparing the results obtained from the isolated components with those in the full configuration, thereby determining the installation effects. Although the fairings of the struts on which the propellers were mounted can be considered as wings, their influence was not explicitly considered. In addition to the wind-tunnel campaign, numerical simulations were performed, to assist in the investigation of the phenomena related to the interactions. Given the complexity of the configuration and the large quantity of test conditions, high-fidelity CFD simulations would have proved prohibitive. Therefore, the mid-fidelity code DUST [27] was employed, which is particularly suited for the simulation of the interactional aerodynamics of rotary wings.

2. Experimental set up

2.1. Test rig

In this section, the mechanical components of the test rig are described, while in Section 2.2 the measurement system is detailed. Since the interest of the study was chiefly in the interaction between the rotors, only the main rotor and the propellers were considered, without modelling the fuselage (Fig. 1).

2.1.1. Main rotor

The main rotor model is constituted by the LHD Wind Tunnel Rotor Rig, made available by Leonardo Helicopters. The rig is composed of a vertical pylon, on which all the kinematic mechanisms, actuators, and electronic devices necessary to the operation of the rotor and the transmission of the signals from various measurement instruments are mounted. The pylon is set on a metal support structure, which by using compressed air cushions is able to move on the wind tunnel floor, allowing precise positioning and alignment of the rig. The pylon can be tilted in the forward-aft plane and also rotated around its axis, reproducing the mast inclination and yaw angle of the rotor, respectively. An electric motor, with a maximum power of 160 kW and maximum torque of 500 N m, is installed in the lower rig frame and drives the rotation of the rotor through a transmission shaft housed in the hollow pylon.

The five-bladed rotor head, installed on the top of the pylon, is fully articulated, with hinges for the pitching, flapping, and lead-lagging motion of each blade. Three linear servo-actuators control the movement of the fixed swashplate, which then translates through the rotating swashplate and pitch links into the collective and cyclic pitching motion of the blades. For this study, simple rectangular, untwisted, carbon-fibre blades have been chosen, with a chord of 0.06 m and a NACA 0012 airfoil section, constant along the span. The total rotor radius is 0.858 m, with a root cutout of 0.256 m. Static structural tests, both non-destructive and destructive, were conducted on the blades to determine the main structural properties, considered constant along the span as a first approximation. The main rotor blades geometrical and structural properties are reported in Table 1.

Table 1
Main rotor blade characteristics.

Radius	R_{MR}	0.858 m
Chord	c_{MR}	0.06 m
Root cut-out	-	0.256 m
Mass per unit length	m	0.221 kg m^{-1}
Flexural rigidity	EI	33.2 N m^2
Torsional rigidity	GJ	15.4 N m^2 rad^{-1}
Centre of mass chordwise position	-	40% c_{MR}
Elastic axis chordwise position	-	29% c_{MR}
Airfoil	-	NACA 0012

Table 2
Chord, twist and airfoil section distributions along the propeller blade span.

r/R	chord [m]	twist [deg]	Airfoil
0.24	15.6	24.8	GOE-570
0.32	19.0	15.0	GOE-421
0.39	20.3	9.8	GOE-421
0.47	20.3	6.6	GOE-421
0.55	19.9	4.0	GOE-222
0.62	19.3	2.2	MH-112
0.70	18.5	0.78	GOE-675
0.77	17.5	-0.33	GOE-412
0.85	16.3	-1.07	NACA-4412
0.92	14.9	-1.57	GOE-564
0.97	13.2	-1.40	MH-23
1.00	7.3	-1.24	MH-23

2.1.2. Propellers

Propellers models were the same used for the activities reported in [28,29]. They were designed using off-the-shelf Ramoser varioPROP five-bladed hubs and blades, commonly used for radio-controlled hobby-grade aircraft. The hub is composed of a fixed part and a movable part that can slide inside the former. The blades attach to the latter and are able to rotate around their axis, therefore allowing to change their pitch angle, which is done manually when assembling the hub. In order to avoid undesired movement when operational, shim washers were inserted to constrain the position of the slider and also to allow better control over the pitch setting.

The varioPROP 300-12 blades, available in both right-handed and left-handed configurations, bring the propeller to a radius of 0.15 m. This dimension was chosen in relation to the main rotor size as the will was to reproduce a ratio between main rotor and propeller radii based on a typical compound helicopter machine. In order to characterize the blade geometry, a 3D scan of the blade was acquired and processed to identify both the quantities of interest (chord and twist distribution, coning angle, etc.) and the airfoil sections, which were determined by comparing the actual blade section against a database of common airfoil sections. The propeller characteristics are summarized in Table 2, and more details can be found in [28,29].

Each propeller is spun by a Scorpion HKII-4235-630KV brushless electrical motor, with a maximum continuous power of 5.3 kW. A front spinner was also added and nacelle cowlings were designed and fabricated with the technique of rapid prototyping. No active cooling was implemented, relying instead on slots in the nacelle body to provide passive cooling from the airflow in the wind tunnel. A detailed view of

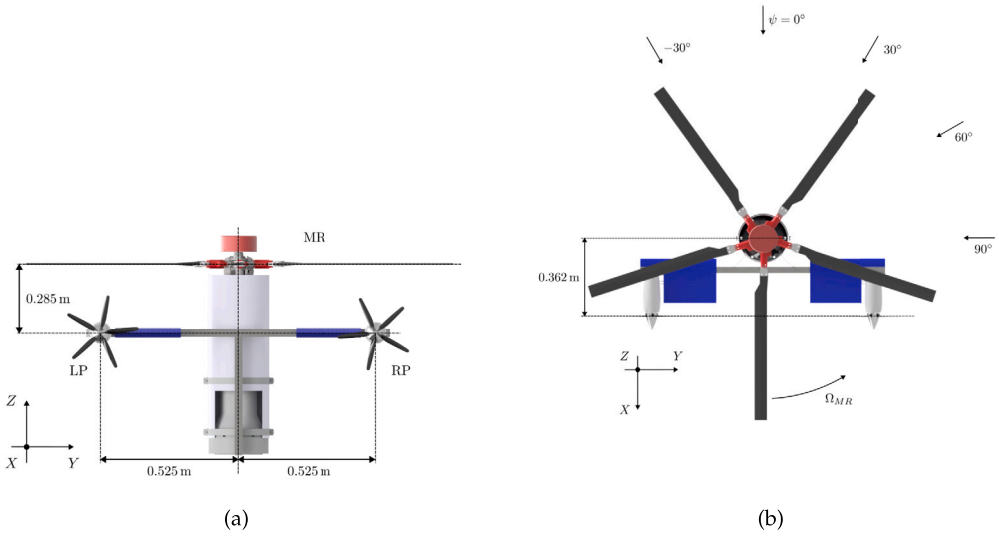

Fig. 2. Schematic of the upper portion of the test rig, including the main rotor (MR), right propeller (RP) and left propeller (LP); the free-stream direction ψ is also indicated. **(a)** view from behind, **(b)** view from above.

the propeller assembly including the main dimensions of the test rig are reported in Fig. 3.

Following a trend in recent compound helicopters, the propellers are mounted in a pusher configuration, i.e. with the propeller behind the motor. Also the propellers' position with respect to the main rotor disk was chosen by similarity to common compound helicopter geometries. In particular, the propellers rotation axes are 0.285 m below the main rotor disk, 0.525 m laterally from the pylon axis on each side and 0.362 m aft the pylon axis. A schematic of the top portion of the test rig is visible in Fig. 2.

The propellers are attached to the ends of a steel "T"-shaped structure, with the stem attached to the rotor pylon and a couple of lateral braces to stiffen the structure. In order to minimize aerodynamic interference, the horizontal part of the structure is covered by 3D-printed fairings with a NACA 0018 airfoil section, which can also be seen as modelling the wings commonly found in compound helicopter concepts. Two Scorpion Tribunus II 06-120A Electronic Speed Controllers (ESCs) are employed to control the motors, characterised by a maximum continuous current of 120 A. The ESCs are mounted on the "T"-shaped structure relying on the metal structure itself and on the external airflow for passive cooling. A custom LabView program was developed to control the motors via Pulse-Width Modulation (PWM) technique. Both the control of the motors and the acquisition of the signals from the load cells were realized through National Instruments compactDAQ modules.

2.2. Measurement instrumentation

The main interest of this study was the measure of the effects of the rotor-propeller interaction on their performance, computed from the aerodynamic loads. The main rotor pylon houses a six-component balance, placed under the static portion of the rotor mast. This balance measures three components of the force and three components of the moment acting on the rotor in a fixed reference frame. Flexible couplings are employed to minimize interference between the balance and the mast and avoid cross-coupling effects, measuring the effective rotor loads. The temperature of the balance is monitored by a thermocouple and an active cooling system can be activated if necessary. The maximum admissible static thrust is 3200 N, with a maximum error of 0.4% of the design load, while for the lateral force components a maximum of 500 N can be reached. The rotor torque is measured by a Kistler torque-meter. Moreover, the main rotor blade cuffs are instrumented with Hall-effect magnetic sensors which allow for the measurement of the pitching, flapping and lead-lagging angles of the blades. For the tests performed in this study, only one blade was instrumented in this way. All the signals from the blade sensors are conditioned by a rotary amplifier and then sent to the acquisition and control system rack via a 100-channel slip-ring.

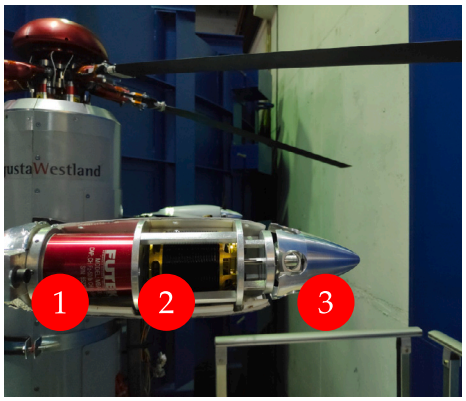

Fig. 3. Detail of the left propeller with the cowling removed: 1 - load cell, 2 - motor, 3 - propeller hub and spinner. The blades are not installed.

For the measurement of the propeller loads, a Futek MBA500 bi-axial load cell is connected to each propeller and housed inside the nacelle (Fig. 3). The load cell can measure thrust up to 223 N and torque up to 5.7 N m (non-linearity ±0.25% Rated Output, hysteresis ±0.25% Rated Output, non-repeatability ±0.05% Rated Output). Passive cooling is employed for the load cells, and the temperature was monitored showing that neither for the motors nor the load cells it reached undesired values during the tests.

2.3. Wind-tunnel

The tests were conducted in the Large Wind Tunnel of Politecnico di Milano (GVPM), a closed-loop wind tunnel with a test-section of 4 m by 3.84 m and a maximum speed of 55 m s^{-1}, with a maximum turbulence level of 0.1%. The wind tunnel was used in the open test-section configuration, with the rotor rig placed in the middle of the test section (Fig. 4) and accurately positioned with respect to the tunnel axis by employing a laser alignment system.

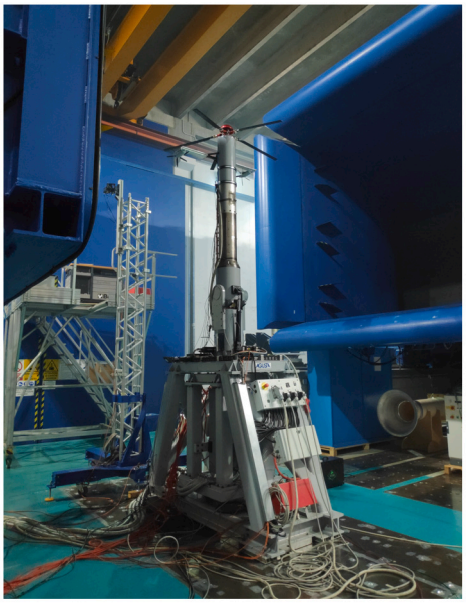

Fig. 4. Complete rig in the wind tunnel, with the rotor pylon yawed to achieve the condition $\psi = 90°$. The air flow is from left to right in the image.

It is known that the estimation of wind-tunnel corrections in the case of a rotor in an open test-section can be challenging. While some indications can be found in literature, for example in [30], the unusual configuration of the present test model, which features two propellers in addition to the main rotor, would add further complexity to the analysis. In the present work, therefore, it was chosen not to apply any kind of wind tunnel corrections to the measured experimental data. This choice was also motivated by the fact that the main interest of the study is in the interactional behaviour, which is determined by comparison and on which wall interference would have only a weak effect.

2.4. Test conditions

In order to study the installation effects, that is, the effects of the interactions between main rotor and propellers, different combinations of the components were tested:

- the main rotor only (referred to as "MR");
- the main rotor with only the right propeller active ("MR+RP");
- the main rotor with both right and left propeller active ("MR+RP+LP").

The choice of prioritising the right propeller was due to the fact that, given the test conditions, as described below, the left propeller would operate in an unfavourable environment. When a propeller is not indicated as active, it is to be intended that only the blades were removed, while nacelles, spinners and fairings were present at all times.

For each of the above combinations, different flight conditions were considered, in terms of wind direction and speed, as summarized in Table 3. In particular, low to moderate advance ratios μ, ranging from 0 (hovering flight) to 0.1 were considered, where $\mu = \frac{V_\infty}{V_{tip}}$, with V_∞ being the wind-tunnel speed and V_{tip} the speed of the tips of the main rotor blades. In addition, the rotor pylon was rotated to have different yaw angles ψ, ranging from $-30°$ to $90°$ (positive starboard), representing lateral gusts and/or lateral flight of the aircraft. These values were chosen to highlight the interaction of the main rotor wake with the right propeller. The inclination of the pylon, corresponding to the shaft angle of the rotor, was fixed at $0°$.

For the main rotor, Mach-number scaling was sought and a rotational speed of 2200 RPM was chosen, corresponding to a tip Mach number $Ma_{tip,\,MR} = 0.58$. The main rotor was trimmed for a collective pitch angle of $7°$ and a cyclic pitch setting to achieve zero-flapping conditions. Only for the case of $\mu = 0.1$, the collective pitch was set to $6°$, to keep a thrust value similar to that of the other cases.

The propellers' trim condition was chosen considering an anti-torque action, i.e. with the torque generated from the propellers' thrust acting to counteract the reaction torque of the aircraft from the main rotor rotation. This trim strategy is to be intended only as a broad reference condition, and no attempts were made to precisely match the main rotor torque in the different cases. The two propellers are thus differentiated as follows. The right propeller is set to generate thrust towards the front of the aircraft, while the left propeller is set to generate thrust towards the rear of the aircraft. While both propellers are nominally in a pusher configuration, i.e. positioned after the engine, in the following the term "pusher" will be used to describe a propeller generating thrust towards the front (e.g., the right propeller). The rotational speed of the propellers was controlled by the PWM to a nominal value of 8300 RPM and the blades were adjusted to a nominal pitch of $23°$ at the section placed at the 75% of the radius; these conditions were chosen as they were withstandable by motor and ESC for a sufficient time. Given this setup, it was not possible to phase the motion of the propellers between each other, nor with the main rotor, but this was not considered critical. The propellers were spun inboard-side up, but in order to assess any effect of the rotational direction, a separate combination of conditions, referred to as "RP CCW" and "MR+RP CCW", was performed with the right propeller spinning outboard-side up, i.e. counter-clockwise when looking from behind. Moreover, for the case of the highest advance ratio in forward flight $\mu = 0.1$, $\psi = 0°$, an additional condition was tested, namely with both propellers in a pusher configuration, in the sense described above, which would be more realistic for an aircraft in these flight conditions. These latter related combinations are referred to as "RP+LPP" and "MR+RP+LPP".

For the tests considering only the right propeller, a higher nominal rotational speed of 9300 RPM was chosen in order to increase the propeller's tip Mach number to a more realistic value. The wind direction corresponding to ψ =-30° was not included in these tests, owing to the fact that the propeller would be affected by the wake of the test rig components. In order to make a comparison with the cases with both propellers active, an additional series of tests was performed again with only the right propeller, but spinning at 8300 RPM (referred to as "RP SLOW" and "MR+RP SLOW"). This also allowed to evaluate the influence of the rotational speed on the interaction effects.

For the tests with main rotor and propellers operational, the propellers were kept spinning at a lower speed (close to 5000 RPM) and then brought up to the nominal speed only for a time of 10 s, during which both main rotor and propeller instrumentation signals were acquired. This was done to avoid overheating the ESCs and causing an emergency stop. It is important to notice that the main rotor trim was adjusted with the propellers running at the lower speed mentioned, and was not modified as the nominal speed was reached. For the tests with only the propellers operational, since the main rotor could not be left unpowered in the active wind tunnel for safety reasons, it was kept rotating at a lower speed of 1100 RPM and with a collective pitch setting close to $0°$. In these conditions, a very low thrust was generated and it could be considered as if the propellers were not influenced by the presence of the rotor.

A summary of all test series and conditions is available in Table 3.

2.5. Data reduction

The main indicators examined, for the main rotor and the propellers, are the thrust coefficient C_T, the torque coefficient C_Q and the efficiencies FM and η. In this context, thrust is defined as the component of the aerodynamic force directed along the axis of rotation.

When presenting the results below, the installation effects are reported as the relative difference in the coefficients, accompanied by the

Table 3
Test conditions as combination of advance ratio μ, wind direction ψ, and rotational velocity of each component.

Name	μ	ψ	Nominal RPM			Notes
			MR	RP	LP	
MR	0, 0.025, 0.05	0°, 30°, 60°, 90°	2300	-	-	
	0.1	0°	2300	-	-	
RP+LP	0, 0.025, 0.05	0°, 30°, 60°, 90°	-	8300	8300	$\theta_{LP} = 22°$
	0.1	0°	-	8300	8300	
MR+RP+LP	0, 0.025, 0.05	0°, 30°, 60°, 90°	2300	8300	8300	$\theta_{LP} = 22°$
	0.1	0°	2300	8300	8300	
MR+RP+LPP	0.1	0°	2300	8300	8300	LP pusher
RP	0, 0.025, 0.05	0°, 30°, 60°, 90°	-	9300	-	
	0.1	0°	-	9300	-	
MR+RP	0, 0.025, 0.05	0°, 30°, 60°, 90°	2300	9300	-	
	0.1	0°	2300	9300	-	
RP CCW	0, 0.025, 0.05	0°, 30°, 60°, 90°	-	9300	-	RP counter-clockwise, $\theta_{RP} = 22°$
	0.1	0°	-	9300	-	
MR+RP CCW	0, 0.025, 0.05	0°, 30°, 60°, 90°	2300	9300	-	RP counter-clockwise, $\theta_{RP} = 22°$
	0.1	0°	2300	9300	-	
RP SLOW	0, 0.025, 0.05	0°, 30°, 60°, 90°	-	8300	-	
	0.1	0°	-	8300	-	
MR+RP SLOW	0, 0.025, 0.05	0°, 30°, 60°, 90°	2300	8300	-	
	0.1	0°	2300	8300	-	

indication of the two conditions being compared: as an example, concerning the main rotor thrust, the wording "MR+RP vs MR" refers to the difference between the case with main rotor and right propeller active and the case with only main rotor active, i.e.

$$\Delta C_{T,MR} = \frac{C_{T,MR}\big|_{MR+RP} - C_{T,MR}\big|_{MR}}{C_{T,MR}\big|_{MR}} \tag{1}$$

Each test point was repeated three times, and the results averaged; no significant drift of the measurements was recorded. The measured loads covered approximately 25% and 25%–30% of the available range for the main rotor and the propellers, respectively. The uncertainties on the coefficients defined above were estimated to be less than 0.5% for what concerns the main rotor, and less than 1% for what concerns the propellers.

2.6. Numerical simulations

For the numerical simulation of the experimental tests, the in-house, open-source, mid-fidelity aerodynamic code DUST [31] was employed. The main rotor and the propellers' blades were modelled using lifting-line elements, with a discretisation of 22 and 30 panels span-wise, respectively. Aerodynamic data for the airfoil sections were computed using XFOIL and extending the results over the entire range of incidences according to the procedure detailed in [32]. The propellers' nacelles were also included in the simulations, as non-lifting bodies. The rotor pylon and the fairings were not modelled, to reduce the computational effort.

A critical issue to tackle was related to the main rotor blade torsional deformation. From preliminary computations on the main rotor in hovering conditions, an underestimation of the generated thrust was highlighted. As the torsional deformation of the blades was identified as a candidate to explain this discrepancy, simulations taking into account the structural properties of the main rotor blades were performed employing the aeroelastic suite, featuring the coupling between DUST and MBDyn, a multibody dynamics solver [33]. The coupled simulations, utilising the non-linear vortex-lattice element [34], showed that the discrepancy was removed for the hovering rotor and that the blades indeed presented torsion, which increased the local incidence and thus the generated loads. However, the approach followed in this work was to extract the torsion span-wise distribution from the aeroelastic simulations of the main rotor alone and to introduce it as an equivalent twist of the blades in purely aerodynamic simulations of all the cases, performed with DUST. This method does not ensure precise agreement with the experimental values, given that the actual torsion distribution varies in time, while the equivalent twist description is constant and computed as an average over a revolution. However, this was considered adequate for the purpose of gaining a better understanding of the aerodynamic interactional behaviour providing a better understanding of the insights obtained by load measurements.

Given the vast number of conditions tested, only a few were selected to be reproduced numerically. In order to assess the effects of the interactions, separate simulations for each isolated component were also performed and compared to the full configuration, mimicking the experimental test campaign. A total of 32 propeller revolutions and, correspondingly, 8 main rotor revolutions were simulated for each selected test case, taking about 2 hours on a workstation-level computer. Such a length was deemed sufficient for reaching a steady-like state, although the phenomena related to the interactions, in particular the wake tip vortices convection, introduced time scales with a longer periodicity.

3. Results and discussion

3.1. Full configuration

In this section the experimental results for the full configuration, consisting of main rotor and both lateral propellers, are presented.

3.1.1. Main rotor

In Fig. 5 the variation of the main rotor thrust and torque coefficients with respect to the wind direction ψ is shown for the two advance ratios considered. The results for the main rotor alone show no dependence on the wind direction, which is expected given that the rotor is trimmed for

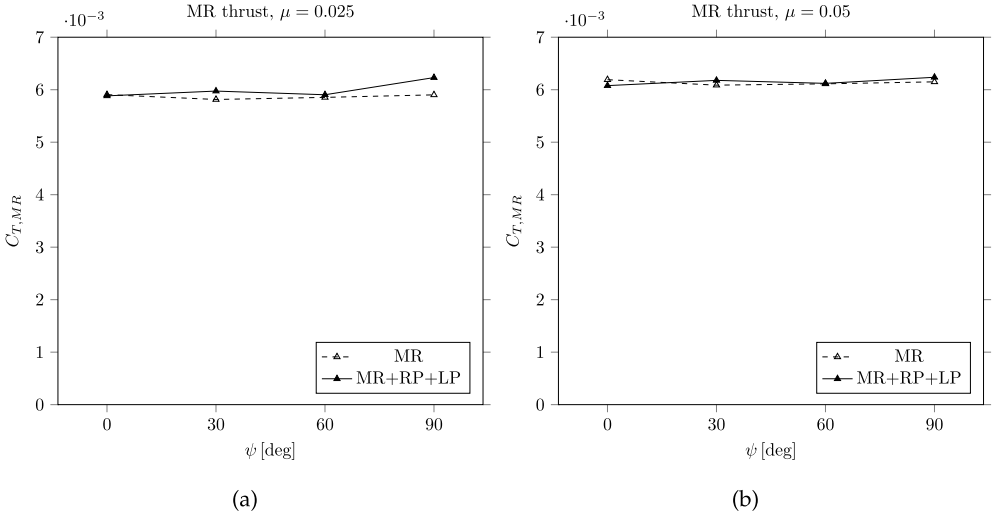

Fig. 5. Main rotor thrust coefficient variation with wind direction; the cases with only the main rotor active (MR) and with main rotor and propellers active (MR+RP+LP) are compared for the two advance ratios.

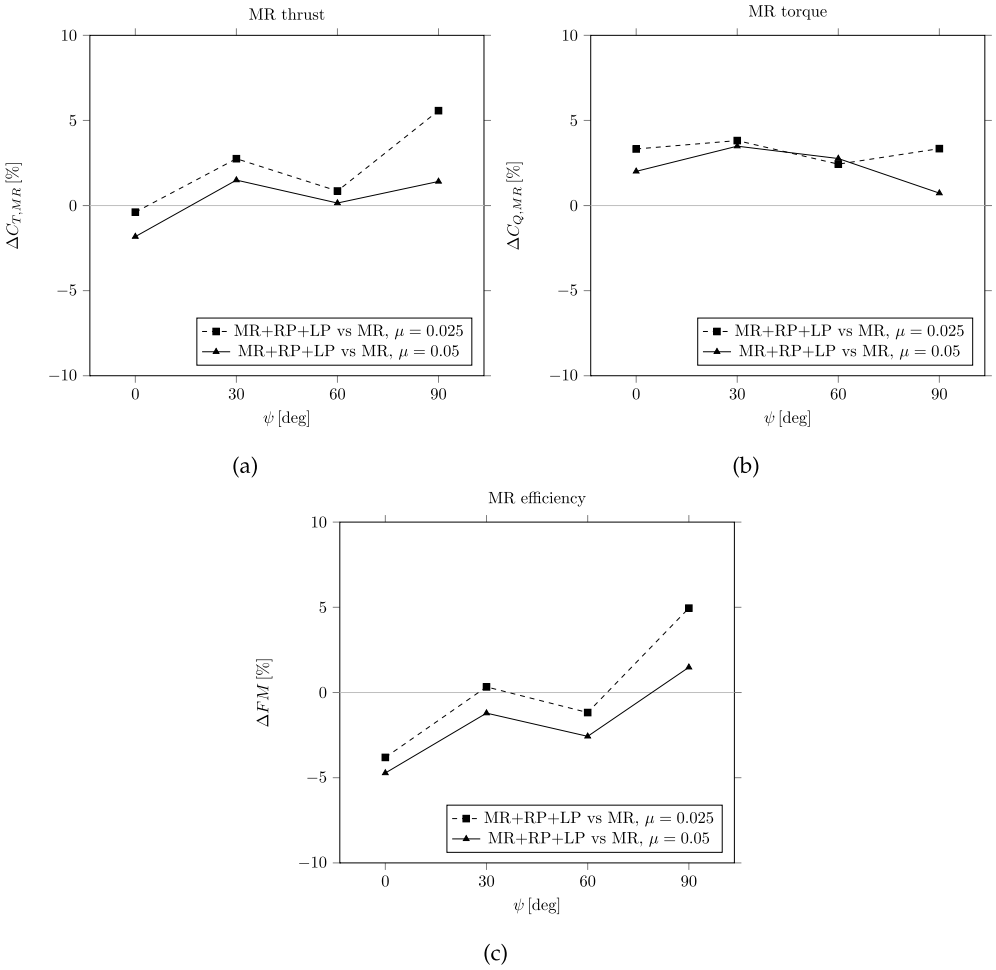

Fig. 6. Installation effect on thrust, torque, and efficiency of the main rotor; the cases with only the main rotor active (MR) and with main rotor and propellers active (MR+RP+LP) are compared.

each condition. By comparing the case with only the main rotor active to that with also the propellers active (Fig. 6), representing the full compound configuration, a variation in the thrust of the main rotor can be seen, with a slight dependence on wind direction. Except for the case of $\psi = 0°$, this variation leads to a small increase of the generated thrust, up to a maximum of 5.6% for $\psi = 90°$ and $\mu = 0.025$. This behaviour can be associated with a blockage effect by the propellers' wakes, and, in the latter condition, could be related to the fact that the right propeller

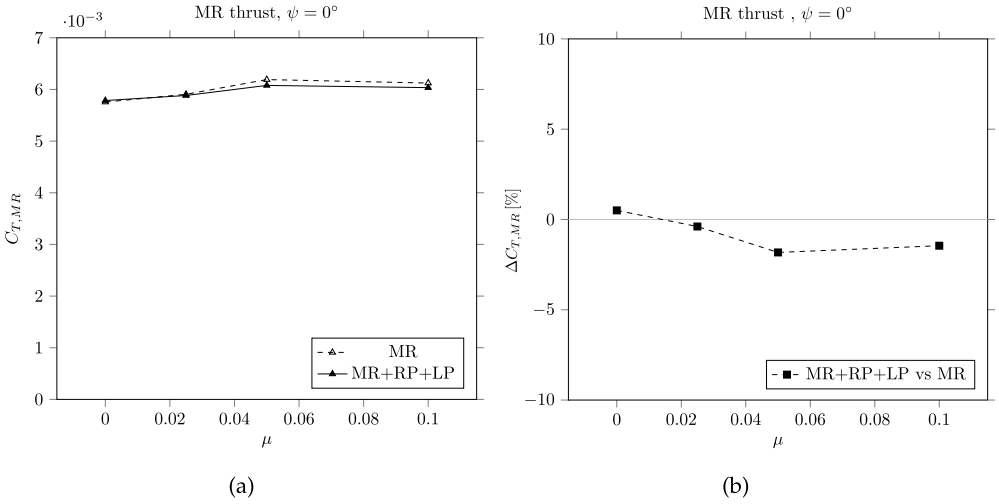

Fig. 7. Main rotor thrust coefficient variation with advance ratio (left) and installation effect on main rotor thrust (right); the cases with only the main rotor active (MR) and with main rotor and propellers active (MR+RP+LP) are compared.

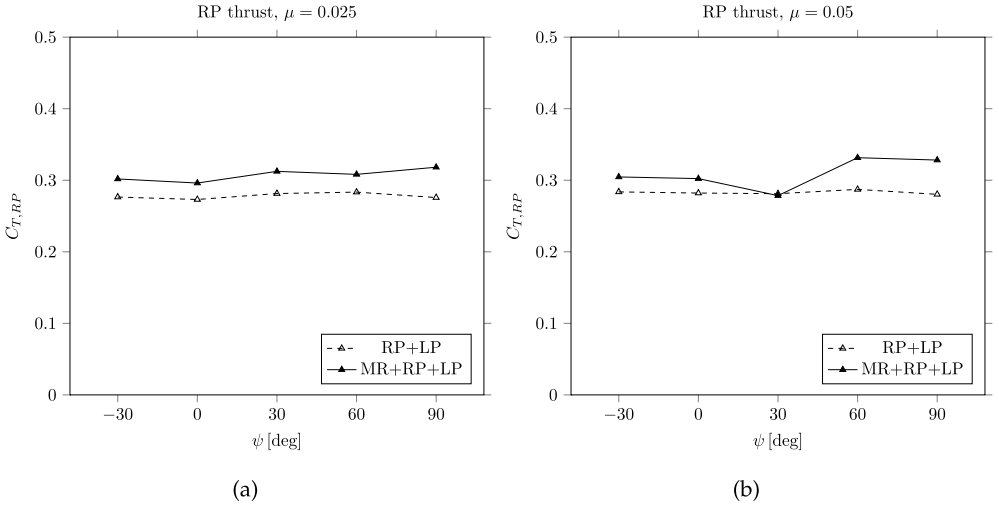

Fig. 8. Thrust coefficient variation with wind direction for the right propeller; the cases with only the propellers active (RP+LP) and with main rotor and propellers active (MR+RP+LP) are compared.

wake is convected to a greater extent directly under the main rotor disk; it is difficult, however, to generalise this statement to the other conditions from these data alone, taking into account also the left propeller. The required torque also increases by around 3% for almost all cases, which entails a slight reduction in the main rotor efficiency. These observations are in agreement with the ones found in literature, which report a limited influence of the propellers on the main rotor in hovering and forward flight [26,8]: in particular, [26] indicates a contrast between the blockage effect from the propellers' wakes, which tends to locally increase the main rotor blades' incidence, and a suction effect by the propeller in the region in front of them, which conversely would decrease the incidence. In their numerical results, the composition of these two factors leads to a negligible main rotor thrust variation in hovering conditions, while an increase of 2% in thrust is obtained for an advance ratio of 0.05. The present measurement, on the other hand, shows a decrease in thrust for the same condition, but the comparison is made difficult by the difference in the geometry of the models (Fig. 7).

3.1.2. *Right propeller*

By looking first at the thrust of the isolated propellers in Fig. 8, a slight variation with the wind direction is visible, with a small increase for the positive values of ψ with respect to the frontal direction, which is consistent with the reasoning in the above Section 1. The effect is less evident for ψ =-30° since in this condition the right propeller is in the wake of the pylon.

The installation effect on the right propeller, as also seen from Fig. 9 and 10, is much more consistent than that on the main rotor. For $\mu = 0.025$, the thrust generated by the propeller shows a consistent and significant increase of around 10%, with a peak of 15.4% for $\psi = 90°$. The same general behaviour can be observed also for the higher advance ratio, with an increase reaching 17%, but an exception in the behaviour is clearly noticeable for the condition $\mu = 0.05, \psi = 30°$. In this case, not only does the thrust of the propeller not increase, but it decreases by about 1% with respect to the case with the propellers alone.

The effect of the main rotor's downwash is therefore an evident increase in the generated thrust, as expected. The magnitude of this influence, with respect to the variation induced on the propeller alone by the oncoming wind-tunnel free-stream, is consistent with the estimate of the downwash velocity. In particular, the highest increases recorded for $\mu = 0.5$ and for the later wind directions can be explained by the fact that in these conditions the propeller would be only partially immersed in the main rotor wake, and, specifically, only the inboard side would be influenced by the downwash, while the balancing effect from the outboard side reducing the thrust would be absent.

These findings are in agreement not only with the remarks mentioned in Section 1, but also with the numerical results by [5,9,26,8,11],

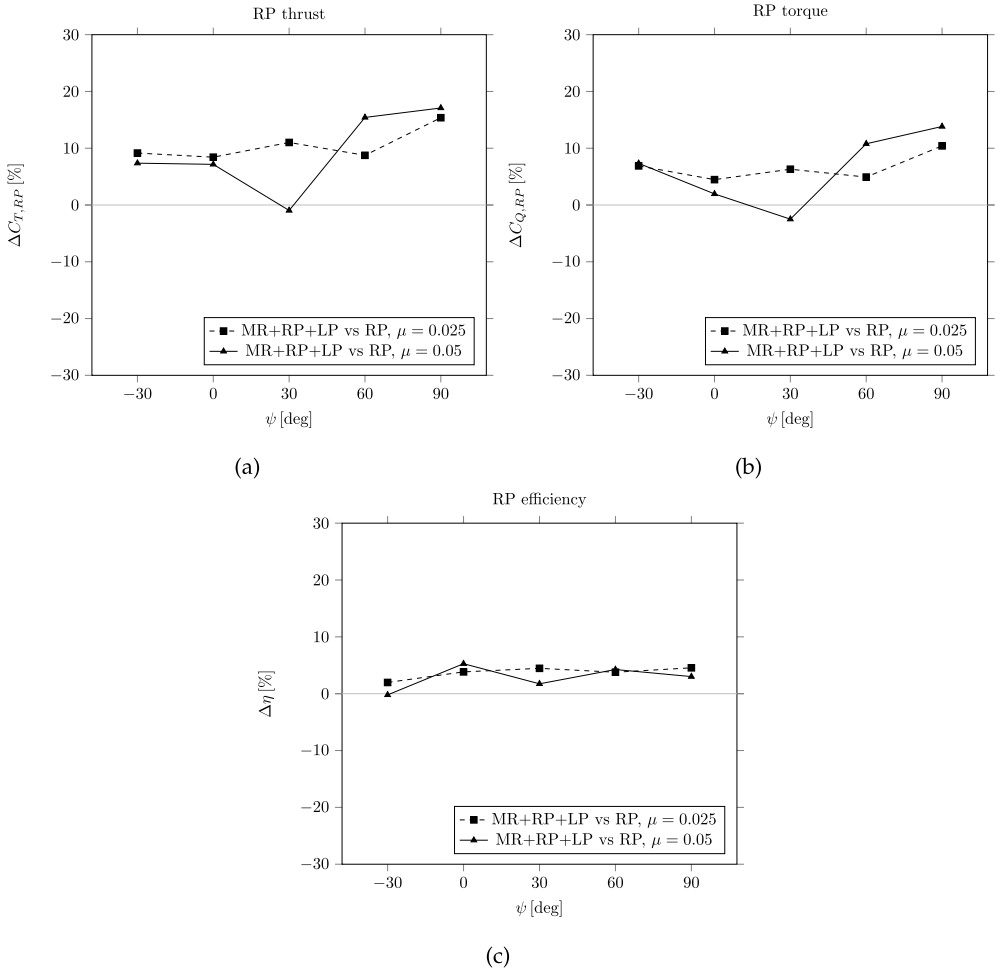

Fig. 9. Installation effect on thrust and torque of the right propeller; the cases with only the propellers active (RP+LP) and with main rotor and propellers active (MR+RP+LP) are compared.

which, considering only hovering or forward flight conditions, report a positive thrust gain as a result of the interaction with the main rotor. Despite the somewhat different aircraft configurations, there is generally quite a good agreement also quantitatively, with the increase being in a range of 7%–10%. This remains true, however, if only the main rotor and the lateral propellers are considered. As reported by [8], the effect of the wings can be drastic, and even result in an ultimately negative installation effect. In comparing with other works in literature, care must be taken in distinguishing between the two lateral propellers: the anti-torque action is realised by setting one of the propellers to produce reverse thrust, but whether it would be the left one or the right one depends on the direction of the rotation of the main rotor.

Finally, the exceptional behaviour was observed only at $\mu = 0.05, \psi = 90°$ and this locality in terms of advance ratio and wind direction suggests a phenomenon related to the main rotor wake convection as a possible explanation. In particular, it could be related to a BVI event resulting from the tip vortices of the main rotor interacting with the propeller. Other authors have pointed out these interactions [7], although ascribing to them only minor effects. It is likely that the occurrence and the behaviour of a BVI event would be very sensitive not only to the flight conditions and the aircraft geometry, but also to other aspects, such as the propeller's blade aerodynamic characteristics. This would make a comparison of the results particularly difficult, especially when numerical computations are involved, since they might introduce artificial dissipation.

The same observations about the installation effects on the thrust can also be made concerning the propeller's generated torque. The magnitude of the variations, however, is slightly lower than what is measured for the thrust, leading to a general increase in propeller efficiency.

3.1.3. Left propeller

The results of the measurements of the loads of the left propeller are reported in Fig. 11, 12 and 13, from which it is evident for all conditions an increase in thrust, even larger than what observed for the right propeller, reaching up to 35.4% for $\mu = 0.05, \psi$ =-30°. The same reasoning as above, concerning the main rotor downwash, can also be applied here. The larger magnitude of the effect can be attributed to the fact that the propeller is operating in reverse thrust conditions, resulting in higher unfavourable self-interaction with its wake in the isolated condition, which is avoided as the wake is displaced by the main rotor induced velocity. These results are in agreement with those available in the literature, which report a thrust increase on the reverse-thrust propeller by around 20%–25% [5,8].

The slight decline in thrust increase with ψ can be attributed to the left propeller being influenced by the wakes of the other components of the test rig for those wind directions. The propeller's torque also generally increases, but to a lesser extent, resulting in increased efficiency.

3.2. Additional configurations

This section reports the results from the tests on all the additional configurations considered.

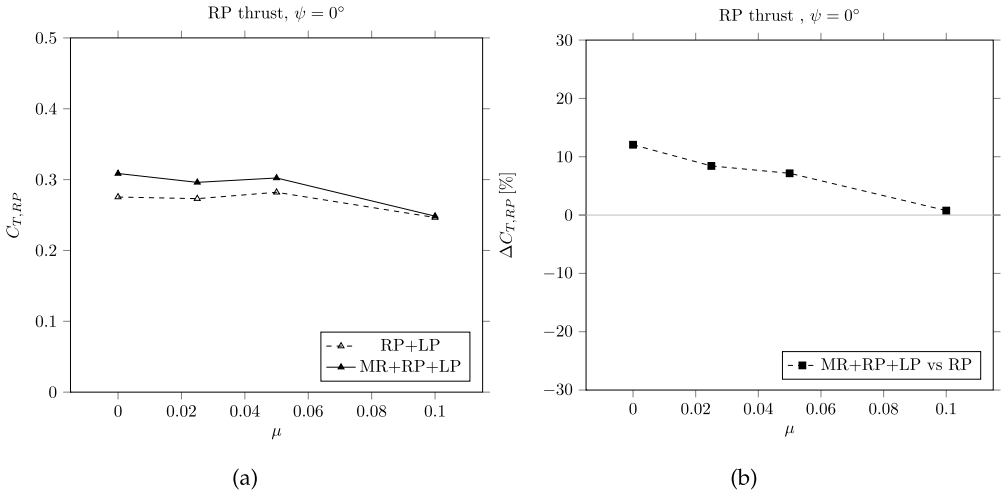

Fig. 10. Right propeller's thrust coefficient variation with advance ratio (left) and installation effect on right propeller thrust (right); the cases with only the propellers active (RP+LP) and with main rotor and propellers active (MR+RP+LP) are compared.

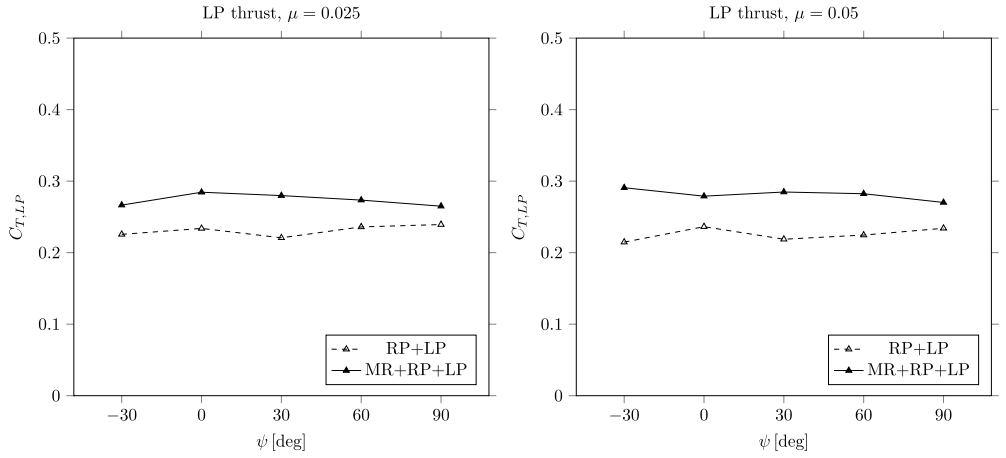

Fig. 11. Thrust coefficient variation with wind direction for the left propeller; the cases with only the propellers active (RP+LP) and with main rotor and propellers active (MR+RP+LP) are compared.

3.2.1. Pusher left propeller

Table 4 presents a comparison of the installation effects between the case with the left propeller in the reverse-thrust operating state and the case with the "pusher" left propeller, tested at $\psi = 0°, \mu = 0.1$. The results show that, while in the former case the propeller experience a noticeable thrust increase as a result of the interaction with the main rotor, in the latter case the installation effect decreases the thrust by 3.2%. This variation can be explained by the fact that, as mentioned above, while in a reverse-thrust regime, the propeller might greatly benefit from the main rotor downwash convecting its wake, as it might prevent vortex-ring state conditions, hence the positive installation effect. When in a pusher configuration, on the other hand, this beneficial interaction is not occurring and, in fact, the resultant behaviour is very similar to that of the right propeller, which presents a decrease in thrust of −3.6% in this condition. This latter value is different from the slightly positive installation effect reported in Fig. 9 for the right propeller in the same flight conditions, which could suggest the influence of the left propeller's wake, which would have a very different evolution in the pusher configuration compared to the reverse-thrust operating state.

3.2.2. Right propeller only

Fig. 14 presents the results for the installation effects on the right propeller, in the cases with only the main rotor and the right propeller involved. The propeller was spun at a nominal rotational speed of 9300 RPM, higher with respect to the cases presented above.

Table 4
Installation effect on thrust, torque, and efficiency of the left propeller; the cases with only the propellers active (RP+LP, and RP+LPP for the pusher left propeller) and with main rotor and propellers active (MR+RP+LP, and MR+RP+LPP for the pusher left propeller) are compared.

	$\Delta C_{T,LP}$ [%]	$\Delta C_{Q,LP}$ [%]	$\Delta \eta_{LP}$ [%]
MR+RP+LP vs RP+LP	+8.3	+0.9	+7.3
MR+RP+LPP vs RP+LPP	−3.2	−3.6	+0.7

The behaviour of the interaction agrees with the previous results for the configuration including both propellers. An overall increase in the generated thrust is observed, although lower in magnitude. This could be explained by the fact that the main rotor downwash velocity is proportionally smaller relative to the propeller's rotational speed, meaning that its influence in determining the relative velocity on the blades and also in displacing the propeller's wake is reduced, compared to the previous case. A drop in thrust of −3.3%, moreover, is again observed for the condition of $\mu = 0.05, \psi = 30°$, which is in agreement with the explanation presented above of it being a BVI effect.

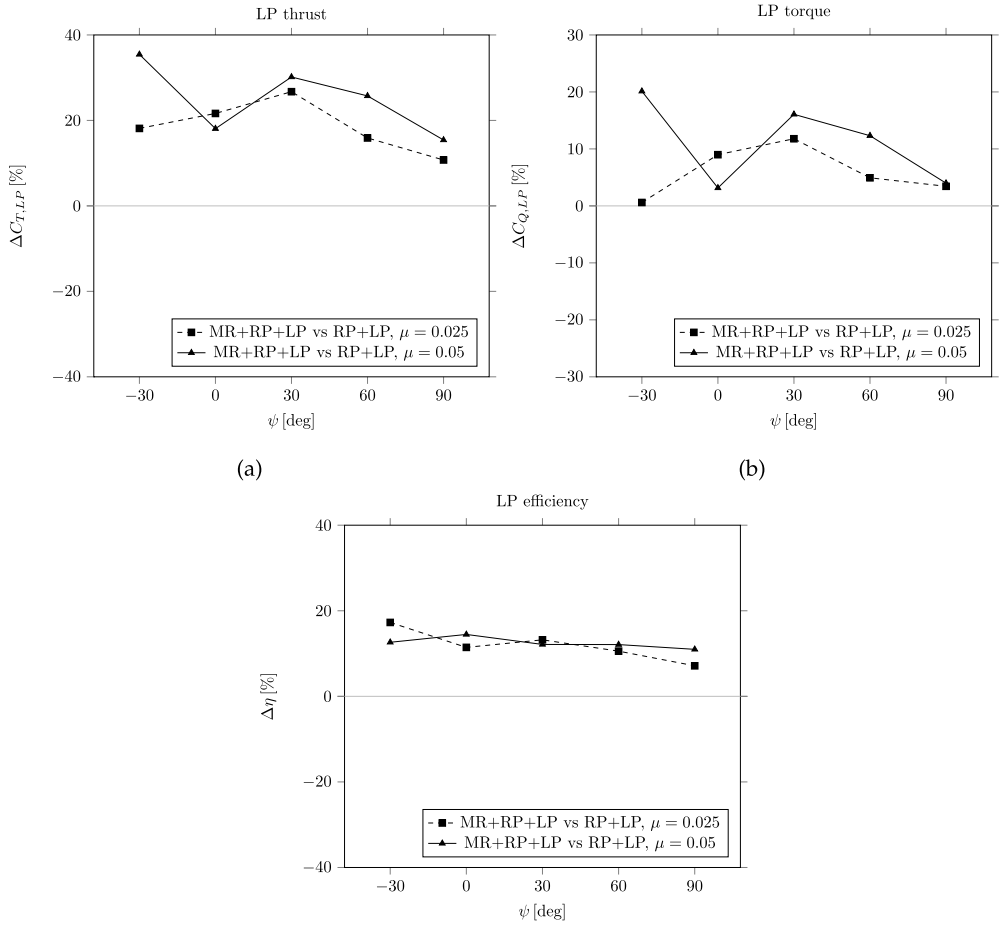

Fig. 12. Installation effect on thrust and torque of the left propeller; the cases with only the propellers active (RP+LP) and with main rotor and propellers active (MR+RP+LP) are compared.

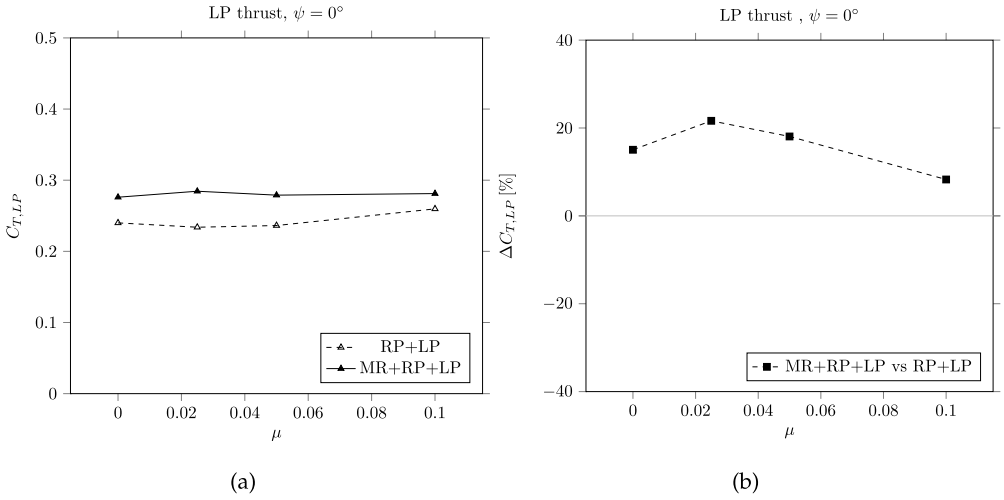

Fig. 13. Left propeller's thrust coefficient variation with advance ratio (left) and installation effect on right propeller thrust (right); the cases with only the propellers active (RP+LP) and with main rotor and propellers active (MR+RP+LP) are compared.

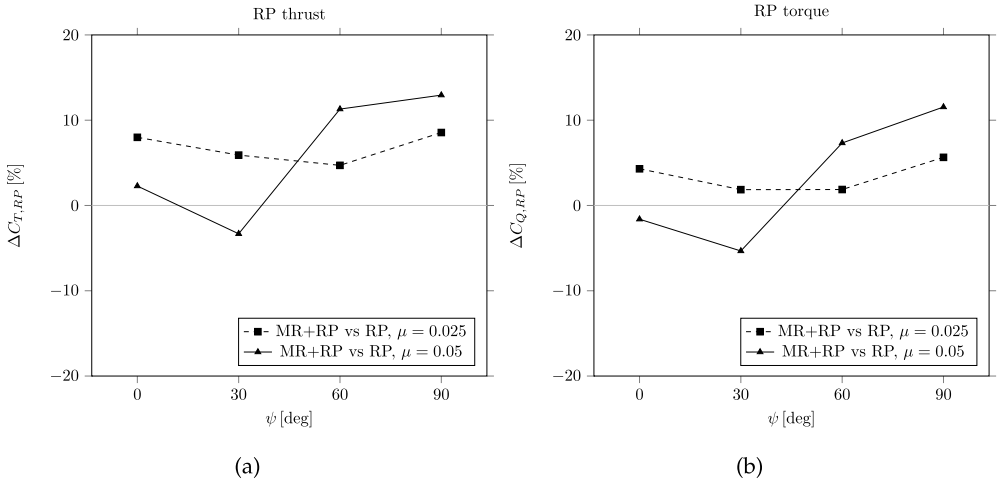

Fig. 14. Installation effect on thrust and torque of the right propeller; the cases with only the right propeller active (RP) and with main rotor and right propeller active (MR+RP) are compared.

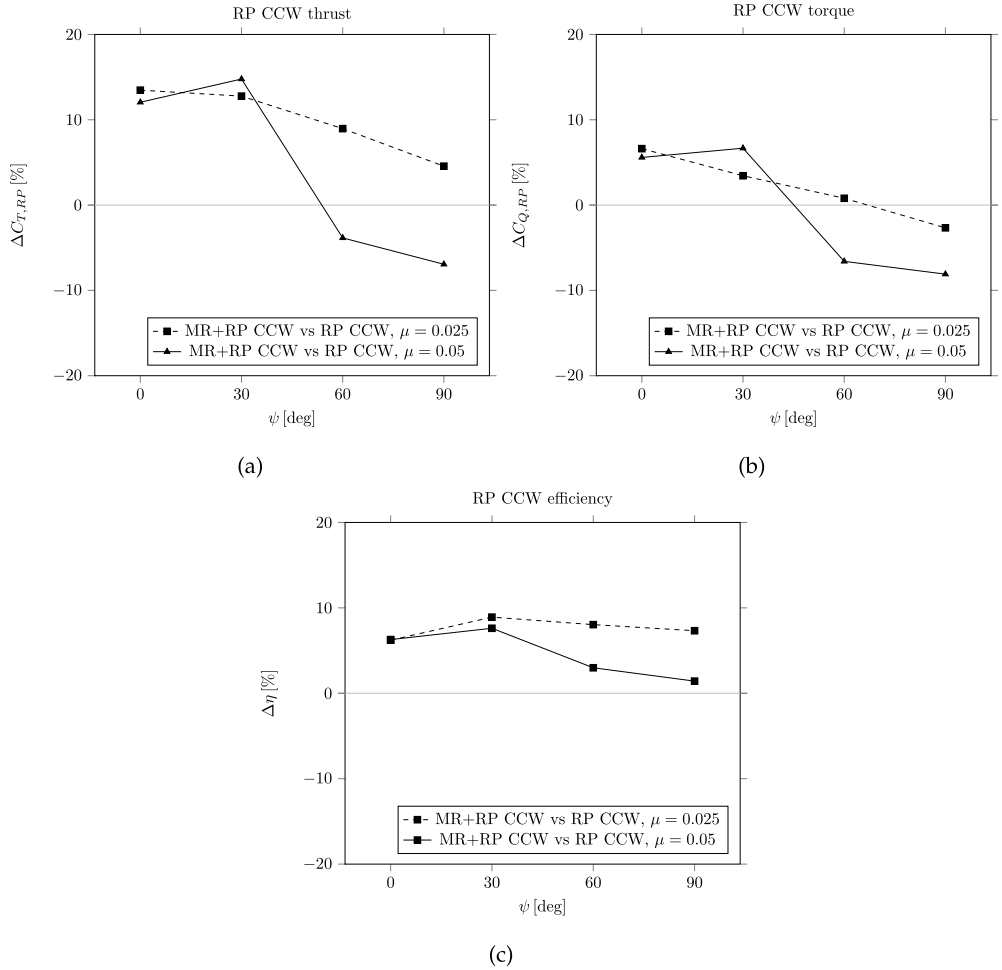

Fig. 15. Installation effect on thrust, torque, and efficiency of the right propeller; the cases with only the right propeller active, and spinning counter-clockwise (RP CCW), and with main rotor and right propeller active, and spinning counter-clockwise (MR+RP CCW), are compared.

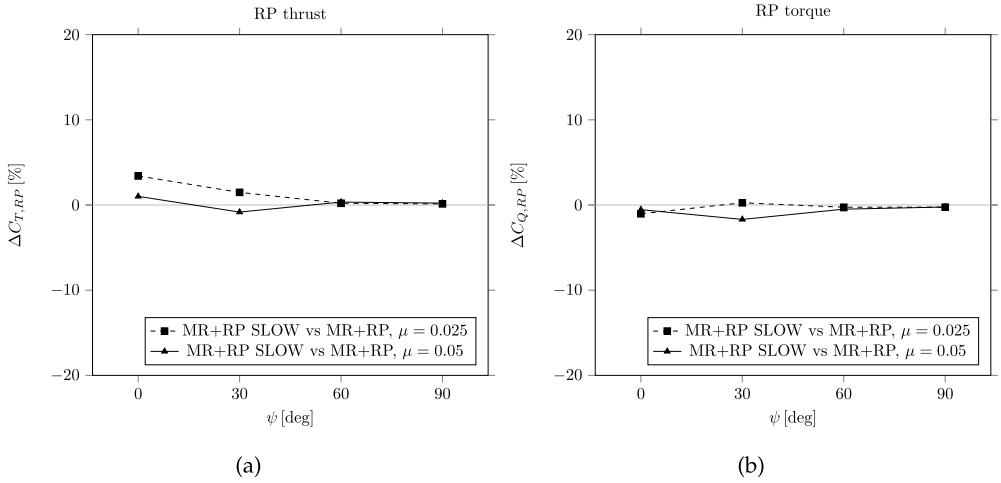

Fig. 16. Installation effect on thrust and torque of the right propeller; the cases with main rotor and right propeller active, and spinning with different rotational speeds, are compared.

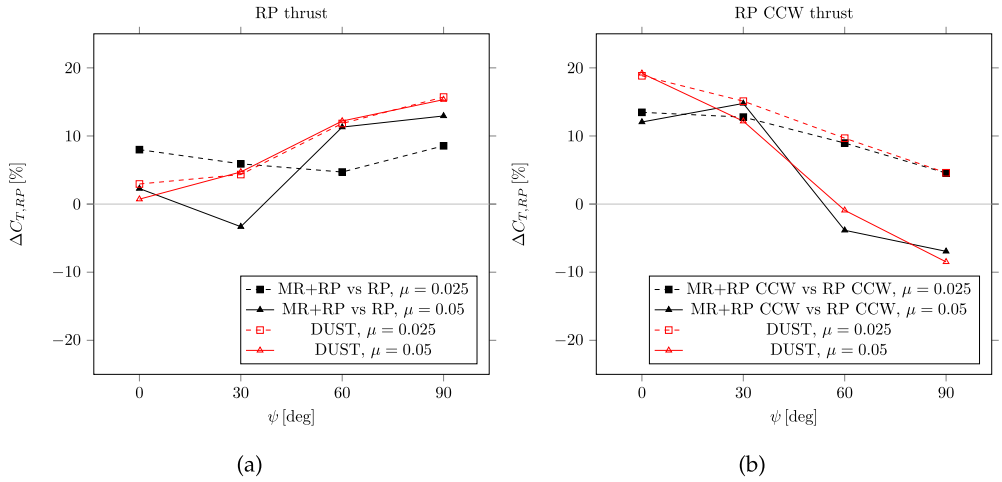

Fig. 17. Results of DUST simulations for the installation effect on thrust and torque of the right propeller; the cases with only the main rotor active and with main rotor and right propeller active are compared. (For interpretation of the colours in the figure(s), the reader is referred to the web version of this article.)

3.2.3. Right propeller spinning counter-clockwise

The results for the cases with the right propeller spinning counter-clockwise are reported in Fig. 15. An increased propeller thrust is observed for $\mu = 0.025$, while for the higher advance ratio the thrust increase for $\psi = 0°$ and 30° is followed by a decrease for $\psi = 60°$ and 90°, to a value of −7%.

When compared with Fig. 14, a certain opposition in the trends can be inferred, which would be consistent with the remarks in Section 1, given the opposite direction of rotation of the propeller. As the propeller is spinning outboard-side up, the composition of the rotational velocity with the main rotor downwash is opposite to that of the clockwise case, while the effect related to the wake displacement would be mostly unaffected, except perhaps concerning the swirl component. The decrease in thrust for $\mu = 0.5$ can again be attributed to the fact that in those conditions the propeller's outboard portion is not fully immersed in the main rotor downwash and therefore the region of favourable interaction would be diminished. Moreover, this same favourable region would be the one most influenced by the main rotor tip vortices, whereas it would be the unfavourable region to be affected in the case of clockwise rotating propeller. Related to this last aspect, the larger increase in thrust for $\mu = 0.05, \psi = 30°$ could be ascribed to the same BVI phenomenon mentioned above, as it is occurring in the same conditions.

3.2.4. Right propeller at different rotational speeds

Fig. 16 reports the difference in the thrust generated by the right propeller, interacting with the main rotor, between the cases with the propeller spinning at 8300 RPM and at 9300 RPM, in order to better highlight the effects of the rotational speed and allow to compare the cases including both propellers with those including only the right propeller It can be seen how the largest difference is 3.4% for $\mu = 0.025, \psi = 0°$, while the differences drop below 1% for the other conditions. This would indicate that the effects of the different rotational speeds are significant only at the lower advance ratio and when the wind direction is such that the propeller's wake is not laterally displaced. These conditions would be the ones for which the effects of the variation in relative velocity induced by the main rotor downwash were more evident with respect to the effects of the wake displacement.

By comparing Fig. 16 with Fig. 14 and Fig. 9, it could be argued that the difference in the installation effect between the MR+RP+LP and the MR+RP cases for the higher values of ψ could be attributed to the presence of the left propeller, since virtually no difference is reported as an effect of the rotational speed for those wind directions. A possible explanation for this influence of the left propeller can be found in the fact that the slipstream of the right propeller, for those values of ψ, is deviated towards the left and could interact with the slipstream of the

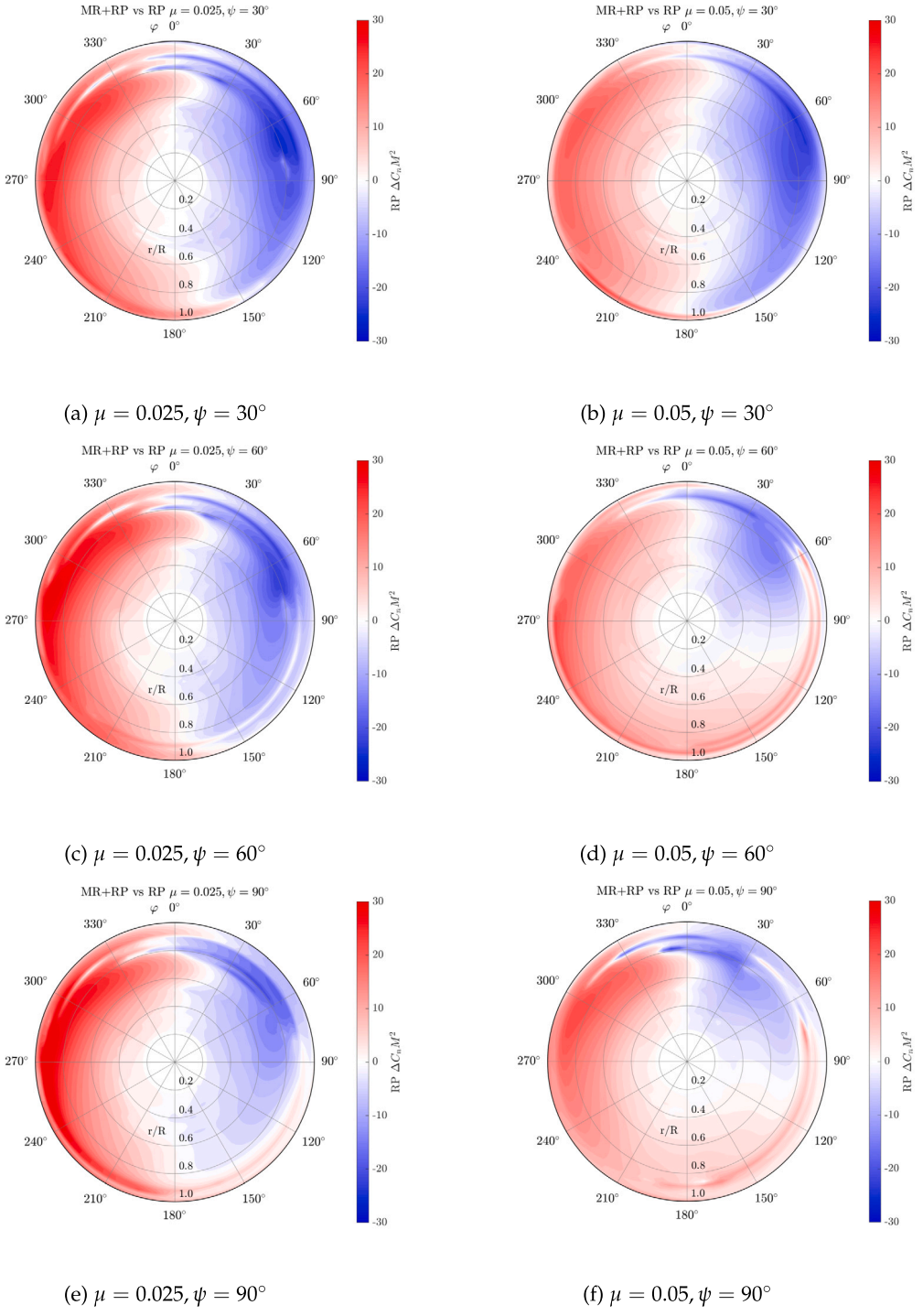

(a) $\mu = 0.025, \psi = 30°$ (b) $\mu = 0.05, \psi = 30°$

(c) $\mu = 0.025, \psi = 60°$ (d) $\mu = 0.05, \psi = 60°$

(e) $\mu = 0.025, \psi = 90°$ (f) $\mu = 0.05, \psi = 90°$

Fig. 18. Distribution over the right propeller's disk of the installation effects in terms of section normal force coefficient, for different flight conditions; view from behind. (For interpretation of the colours in the figure(s), the reader is referred to the web version of this article.)

other propeller, which itself is not deviated as much, being partially shielded by the test rig.

3.3. Numerical simulations

In this section, a selection of the results of the DUST numerical simulations will be presented. Firstly, the general effects of the main rotor downwash on the propeller's loads and load distribution will be examined, while in the second section the behaviour of the main rotor wake, in particular concerning the tip vortices, is shown.

3.3.1. Right propeller

The results from the simulations for the installation effects on the right propeller thrust in lateral wind conditions are presented in Fig. 17 for the MR+RP and MR+RP CCW cases. The reported values are averaged over six propeller revolutions. An agreement with the experimental

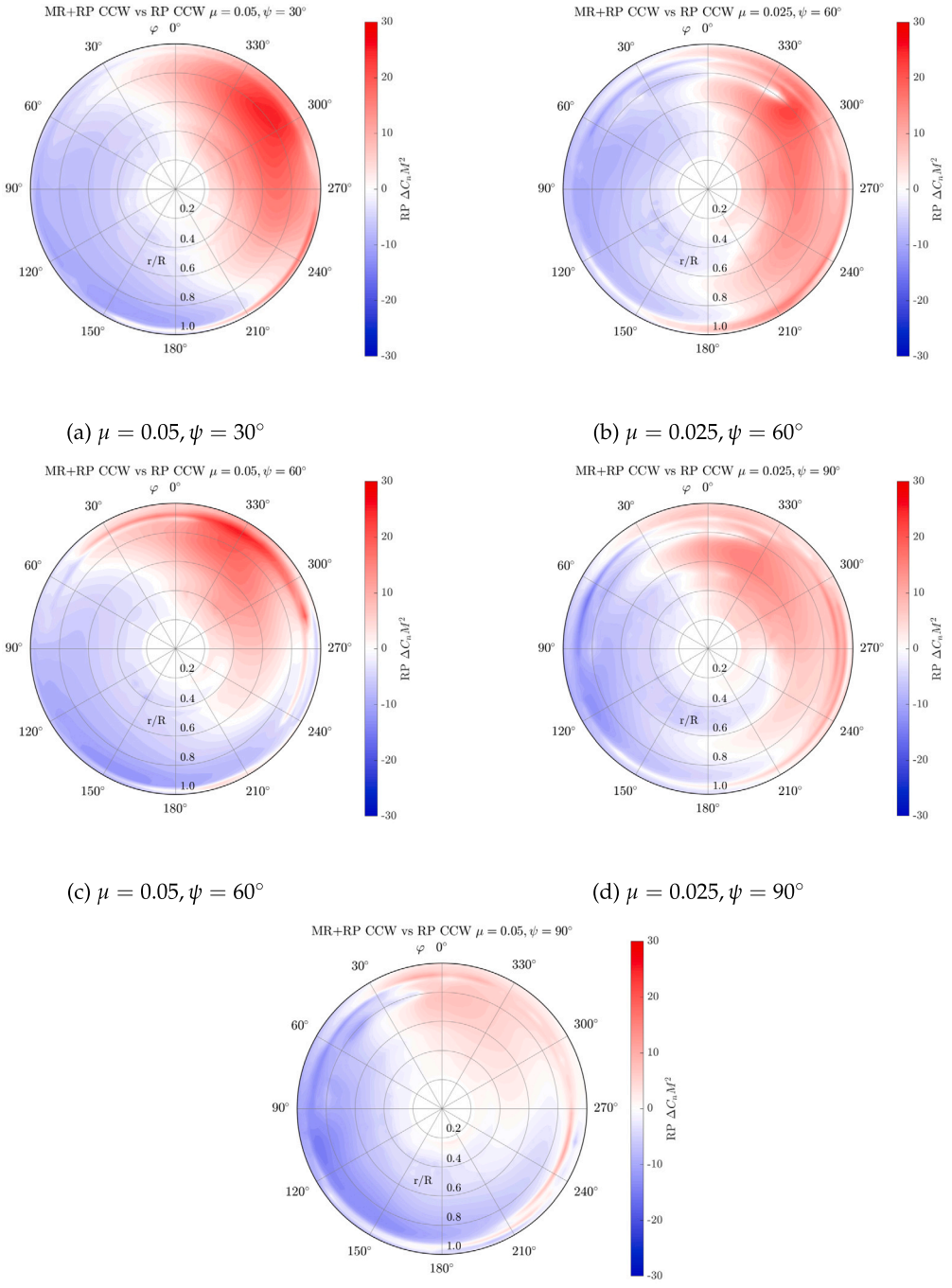

(a) $\mu = 0.05, \psi = 30°$

(b) $\mu = 0.025, \psi = 60°$

(c) $\mu = 0.05, \psi = 60°$

(d) $\mu = 0.025, \psi = 90°$

(e) $\mu = 0.05, \psi = 90°$

Fig. 19. Distribution over the right propeller's disk of the installation effects in terms of section normal force coefficient, for different flight conditions, with the propeller spinning counter-clockwise; view from behind.

results can be seen in terms of general behaviour of the interaction. Discrepancies arise mostly in the case MR+RP for $\mu = 0.05$, where DUST overestimates the thrust increase. This could be a result of issues in reproducing the interaction with the main rotor tip vortices, which would be more significant in those conditions; the same could be said for the case $\mu = 0.025, \psi = 30°$, which was already highlighted as a candidate for important BVI effects. The agreement with the experiments is considerably better for the MR+RP CCW case over all the simulated conditions. This contrast between the accuracy in the two cases might suggest a difference in the interaction with the main rotor wake vortical structures, depending on the direction of the propeller rotation.

The load distribution over the propeller disk, averaged over 10 revolutions, is presented in terms of $C_n M^2$ for different conditions in Fig. 18. In all cases it can be seen how the left side of the disk, corresponding to the upstroking blade, is characterized by an increase in thrust, in particular in the upper portion (azimuth values around $\varphi = 300°$) while the right side shows a decrease in generated thrust with respect to the isolated propeller computation. This is in agreement with the descrip-

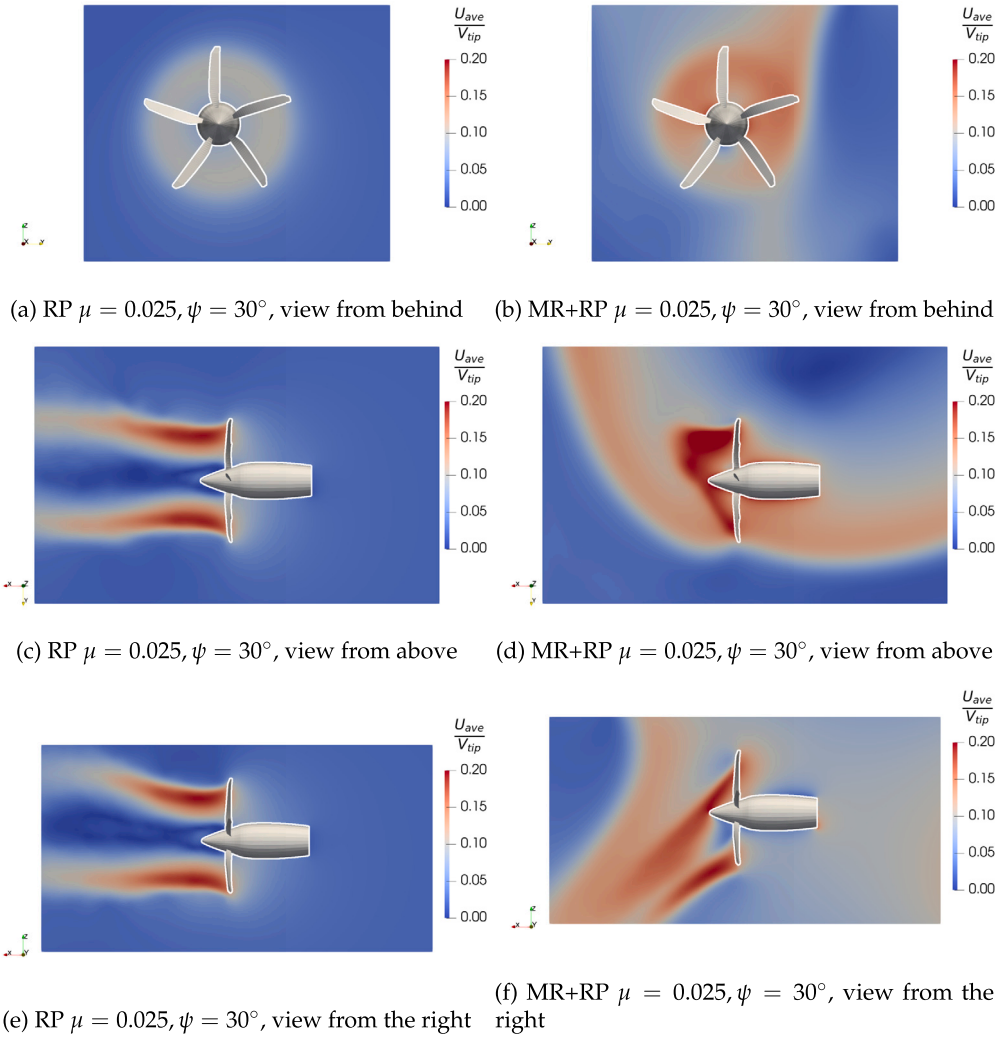

(a) RP $\mu = 0.025, \psi = 30°$, view from behind

(b) MR+RP $\mu = 0.025, \psi = 30°$, view from behind

(c) RP $\mu = 0.025, \psi = 30°$, view from above

(d) MR+RP $\mu = 0.025, \psi = 30°$, view from above

(e) RP $\mu = 0.025, \psi = 30°$, view from the right

(f) MR+RP $\mu = 0.025, \psi = 30°$, view from the right

Fig. 20. Contours of the velocity magnitude averaged over ten propeller revolutions U_{ave}, for the condition $\mu = 0.025, \psi = 30°$; comparison between the case with only the right propeller active (left) and with both main rotor and right propeller active (right).

tion given of the interaction between the propeller and the main rotor downwash. Moreover, as ψ increases, the region of thrust decrease on the right side is reduced, as the main rotor wake is convected inboard, leaving the bottom right of the propeller outside of the downwash area. This is more evident in the case of $\mu = 0.05$, as the wake is more heavily displaced, to the point that for $\mu = 0.05, \psi = 90°$ only a small portion in the upper right of the propeller is adversely affected by the interaction with the main rotor downwash, which is the condition for which the highest thrust increase was measured. Some kinks in the load distribution are visible around $r/R = 0.8$, which can be attributed to the local stalling of the blade, possibly tied to issues in the available aerodynamic data for those sections.

In Fig. 19 the thrust distribution is reported for the RP CCW cases. As expected, the loads increase again over the upstroking portion of the propeller, which is the right side in this case, and decrease over the downstroking region. The main rotor wake displacement for varying μ and ψ is again evident as the favourable interaction zone is restricted to the upper right portion of the propeller's disk, which corresponds to the thrust decrease observed from the experimental results.

3.4. Influence of main rotor downwash

To further illustrate the behaviour of the main rotor wake and the influence of the associated downwash velocity, a selection of flow-field velocity contours is reported in Fig. 20 and Fig. 21, comparing the RP and the MR+RP configurations. The average U_{ave} of the magnitude of the velocity over ten revolutions is shown for three planar sections around the propeller, corresponding to a view from behind (YZ plane), from the top (XY plane), and from the right (XZ plane). In particular, the XY and XZ planes are chosen as the propeller symmetry planes, while the YZ plane is parallel to the propeller disk plane and positioned 0.03 m fore the propeller disk.

The propeller's wake convection by the main rotor downwash is clearly visible in the lateral view, with a region of reverse inflow at the top of the propeller's disk. From the top and front views, it can be seen how the propeller is fully immersed in the main rotor wake, with the boundary of the latter directly touching the rightmost edge of the propeller's disk. Overall, the main rotor wake is only slightly affected by the interaction with the propeller.

The flowfields from the case $\mu = 0.05, \psi = 90°$ show how in this case the propeller's slipstream is already heavily influenced by the lateral free-stream velocity in the isolated case. The main rotor downwash displaces the propeller's wake downward, but from the top view it can be seen how the lateral convection is actually reduced. This can be attributed to the fact that the main rotor wake impacts medially on the propeller, and could provide a sort of blockage effect to the outboard propeller's tip vortices, which are less deflected.

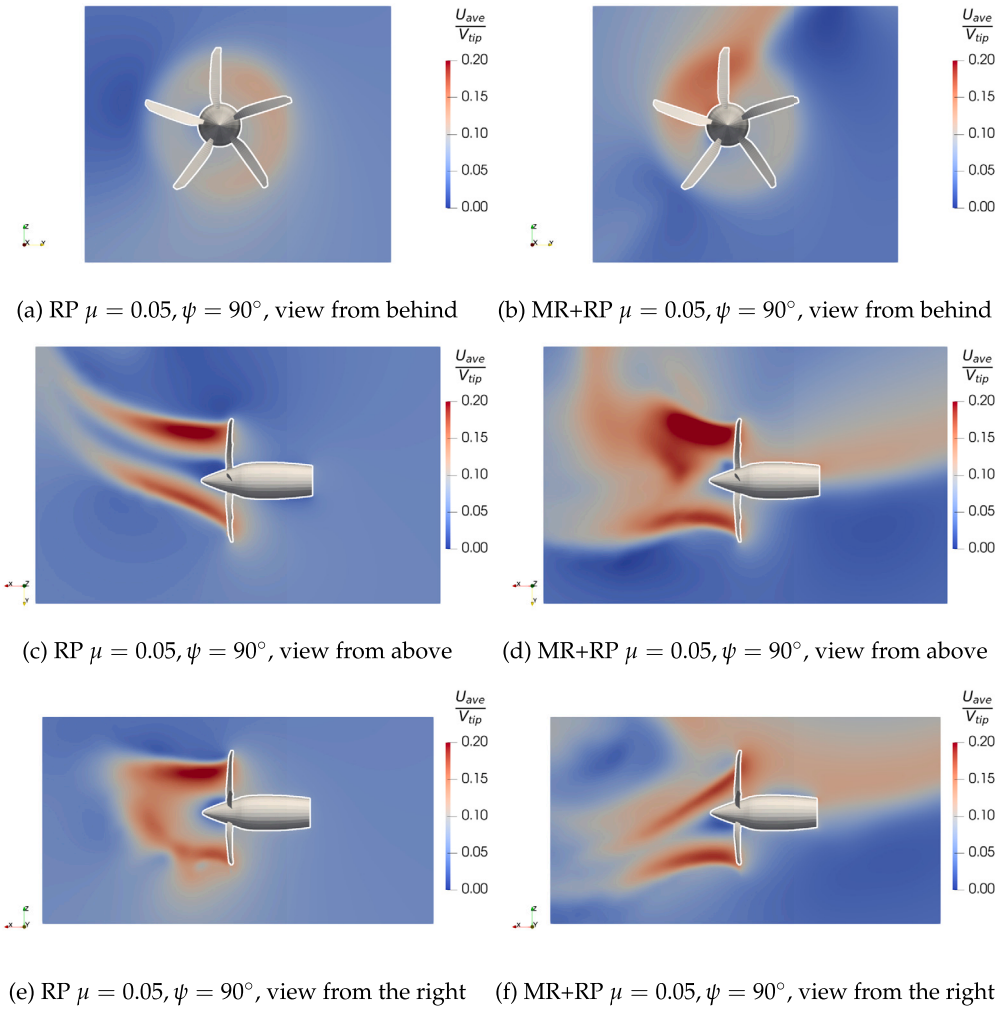

(a) RP $\mu = 0.05, \psi = 90°$, view from behind (b) MR+RP $\mu = 0.05, \psi = 90°$, view from behind

(c) RP $\mu = 0.05, \psi = 90°$, view from above (d) MR+RP $\mu = 0.05, \psi = 90°$, view from above

(e) RP $\mu = 0.05, \psi = 90°$, view from the right (f) MR+RP $\mu = 0.05, \psi = 90°$, view from the right

Fig. 21. Contours of the velocity magnitude averaged over ten propeller revolutions U_{ave}, for the condition $\mu = 0.05, \psi = 90°$; comparison between the case with only the right propeller active (left) and with both main rotor and right propeller active (right).

In general, the flowfields confirm the analysis of the load distribution over the propeller's disk in terms of the position of the main rotor's wake, which is therefore an important parameter to consider when assessing installation effects.

4. Conclusions

The research described in this paper aimed to study the effects of the aerodynamic mutual interference between the main rotor and the lateral propellers of a compound helicopter configuration. For this purpose, an existing rotor test rig was adapted by adding two propeller models and an extensive wind-tunnel test campaign was performed. Thrust and torque measurements of main rotor and propellers were acquired in different flight conditions including hovering, forward and crosswind flight, allowing to evaluate the installation effects on each component.

The results show that the interaction effects on the main rotor are minimal for all the tested advance ratios, with a general slight increase in thrust when the propellers are operational, due to a blockage effect, and a weak variation with the wind direction.

A stronger effect of the interaction is measured on the propellers. There is an important and general increase in the thrust generated, up to 16%, for almost all conditions of advance ratio and wind direction. This increase is attributed to the downwash flow of the main rotor, which introduces a velocity component perpendicular to the propeller's disk, resulting in an asymmetrically distributed load increase. An exception, however, is found for the condition with $\mu = 0.05$ and a wind direction of 30°, where the measured thrust of the right propeller is lower than the value corresponding to the isolated case. This behaviour could be explained by a local effect, such as BVI, although further investigation would be required to confirm the hypothesis. Except for this phenomenon, no qualitative difference was observed between the right propeller and the left propeller behaviours. The latter showed a greater increase in thrust, possibly since, given its operative condition, the main rotor downwash has the beneficial effect of displacing the propeller's wake, avoiding vortex ring state regimes.

The test conducted also allowed to study the influence of the direction and the speed of rotation of the propellers. While the latter did not significantly alter the installation effects, the results for a counter-clockwise right propeller showed an inversion in the trend of the installation effects variation with the wind direction, with a decrease in the propeller's thrust in the case of lateral wind. This behaviour was explained in terms of the main rotor's wake position with respect to the upstroking blade region, which is positively affected by the downwash velocity component.

Finally, numerical simulations with the mid-fidelity aerodynamic code DUST, performed on the configuration including the main rotor and the right propeller, are in qualitative agreement with the experimental results, indicating a thrust increase for the propeller. The simulations

also provided a description of the flow field and of the load distribution on the propeller's disks, from which a clear asymmetry of the generated thrust due to the main rotor downwash can be seen, resulting in the net thrust increase.

In conclusion, in this work experimental evidence is provided of the main rotor downwash resulting in a general significant increase in the thrust of the lateral propellers for a compound helicopter configuration, confirming the findings from similar studies in the literature. While this effect can chiefly be explained as an increase in the local incidence of the propeller's blades, evidence of thrust decrease in particular combinations of advance ratio and wind direction suggests that the vortical structures present in the rotor's wake can play a significant role, which must be taken into account when designing advanced rotorcraft. To this purpose, mid-fidelity numerical tools are found to be useful at least in predicting the dynamics of the structures, if not the effect of the interaction with the blades, which might be more difficult to model, given the importance of viscosity effects.

While this study did not consider a specific aircraft model, nor other components, such as wings, fuselage, and empennage, the effects described are of a sufficiently general nature to be applied to rotorcraft of similar configuration, provided that the conditions are changed accordingly, e.g. for what concerns the flight regime.

CRediT authorship contribution statement

Andrea Colli: Writing – review & editing, Writing – original draft, Visualization, Validation, Software, Project administration, Methodology, Investigation, Formal analysis, Data curation, Conceptualization. **Alex Zanotti:** Writing – review & editing, Supervision, Resources, Project administration, Methodology, Funding acquisition, Conceptualization. **Giuseppe Gibertini:** Writing – review & editing, Supervision, Resources, Project administration, Methodology, Funding acquisition, Conceptualization.

Declaration of competing interest

The authors declare that they have no known competing financial interests or personal relationships that could have appeared to influence the work reported in this paper.

Data availability

The raw/processed data required to reproduce these findings are available upon request to the corresponding author.

Acknowledgements

The authors wish to thank Leonardo Helicopters for the concession to employ the wind tunnel Rotor Rig for the present study, and in particular, for the assistance provided before and during the test phase by their technical staff. Furthermore, the authors acknowledge with gratitude the support of the Aerodynamic Laboratory of Department of Aerospace Science and Technology of Politecnico di Milano. Finally, the authors wish to thank the partners of the GARTEUR HC/AG-25. This work was funded by basic research funding of Politecnico di Milano.

References

[1] M.N. Orchard, S.J. Newman, The compound helicopter — why have we not succeeded before?, Aeronaut. J. 103 (1028) (1999) 489–495, https://doi.org/10.1017/s0001924000064526.

[2] R.A. Ormiston, Revitalising advanced rotorcraft research – and the compound helicopter, Aeronaut. J. 120 (1223) (2016) 83–129, https://doi.org/10.1017/aer.2015.5.

[3] M. Orchard, S. Newman, The fundamental configuration and design of the compound helicopter, Proc. Inst. Mech. Eng., G J. Aerosp. Eng. 217 (6) (2003) 297–315, https://doi.org/10.1243/095441003772538570.

[4] H. Yeo, Design and aeromechanics investigation of compound helicopters, Aerosp. Sci. Technol. 88 (2019) 158–173, https://doi.org/10.1016/j.ast.2019.03.010.

[5] C. Öhrle, F. Frey, J. Thiemeier, M. Keßler, E. Kräamer, Coupled and trimmed aerodynamic and aeroacoustic simulations for Airbus Helicopters' compound helicopter RACER, J. Am. Helicopter Soc. 64 (3) (2019) 1–14, https://doi.org/10.4050/jahs.64.032003.

[6] F. Frey, J. Thiemeier, C. Öhrle, M. Keßler, E. Krämer, Aerodynamic interactions on Airbus Helicopters' compound helicopter RACER in cruise flight, in: Proceedings of the Vertical Flight Society 75th Annual Forum, the Vertical Flight Society, 2019.

[7] J. Thiemeier, C. Öhrle, F. Frey, M. Keßler, E. Krämer, Aerodynamics and flight mechanics analysis of airbus helicopters' compound helicopter racer in hover under crosswind conditions, CEAS Aeronaut. J. 11 (1) (2019) 49–66, https://doi.org/10.1007/s13272-019-00392-3.

[8] F. Frey, J. Thiemeier, C. Öhrle, M. Keßler, E. Krämer, Aerodynamic interactions on Airbus Helicopters' compound helicopter RACER in hover, J. Am. Helicopter Soc. 67 (1) (2022) 1–17, https://doi.org/10.4050/jahs.67.012007.

[9] T. Stokkermans, L. Veldhuis, B. Soemarwoto, R. Fukari, P. Eglin, Breakdown of aerodynamic interactions for the lateral rotors on a compound helicopter, Aerosp. Sci. Technol. 101 (2020) 105845, https://doi.org/10.1016/j.ast.2020.105845.

[10] H. Sugawara, Y. Tanabe, Numerical investigation of rotor/wing aerodynamic interactions at high advance ratios, J. Aircr. 56 (6) (2019) 2285–2298, https://doi.org/10.2514/1.c035370.

[11] K. Kimura, H. Sugawara, Y. Tanabe, Aerodynamic interference between main rotor and side propellers of a winged-type compound helicopter in hover, Trans. Jpn. Soc. Aeronaut. Space Sci. 66 (5) (2023) 174–185, https://doi.org/10.2322/tjsass.66.174.

[12] H.S. Maxim, Screw propellers working in air, Aeronaut. Annu. 1 (3) (1897) 142–144.

[13] D. Riabouchinsky, Recherches sur une hélice mise en rotation dans un courant d'air dirigé perpendiculairement à l'axe de l'hélice, Izv. Ross. Akad. Nauk, Ser. Mat. 24 (1) (1906) 49–52.

[14] H. Glauert, A general theory of the autogyro, Tech. Rep., HM Stationery Office, 1926.

[15] H. McLemore, M. Cannon, Aerodynamic investigation of a four-blade propeller operating through an angle-of-attack range from 0 to 180 degrees, in: National Advisory Committee for Aeronautics Technical Note, NACA, 1954.

[16] R.E. Kuhn, J.W. Draper, Investigation of the aerodynamic characteristics of a model wing-propeller combination and of the wing and propeller separately at angles of attack up to 90 degrees, Tech. Rep., 1956.

[17] P.F. Yaggy, V.L. Rogallo, A wind-tunnel investigation of three propellers through an angle-of-attack range from 0 deg to 85 deg, Tech. Rep., 1960.

[18] B. Ortun, R. Boisard, I. Gonzalez-Martino, In-plane airloads of a propeller with inflow angle: prediction vs. experiment, in: 30th AIAA Applied Aerodynamics Conference, American Institute of Aeronautics and Astronautics, 2012.

[19] D. Serrano, M. Ren, A.J. Qureshi, S. Ghaemi, Effect of disk angle-of-attack on aerodynamic performance of small propellers, Aerosp. Sci. Technol. 92 (2019) 901–914, https://doi.org/10.1016/j.ast.2019.07.022.

[20] T.C.A. Stokkermans, L.L.M. Veldhuis, Propeller performance at large angle of attack applicable to compound helicopters, AIAA J. 59 (6) (2021) 2183–2199, https://doi.org/10.2514/1.j059509.

[21] G. Droandi, G. Gibertini, A. Zanotti, Perpendicular blade–vortex-interaction over an oscillating airfoil in light dynamic stall, J. Fluids Struct. 65 (2016) 472–494, https://doi.org/10.1016/j.jfluidstructs.2016.07.010.

[22] N.M. Chaderjian, Navier-Stokes simulation of UH-60A rotor/wake interaction using adaptive mesh refinement, in: AHS International Annual Forum & Technology Display, No. ARC-E-DAA-TN40776, 2017.

[23] F. Richez, Analysis of dynamic stall mechanisms in helicopter rotor environment, J. Am. Helicopter Soc. 63 (2) (2018) 1–11, https://doi.org/10.4050/jahs.63.022006.

[24] R. Boisard, L. Lefevre, T. Zhang, G. Barakos, A. Visingardi, F. Lößle, A. Kostek, T. Andronikos, M. Keßler, R. Wickersheim, et al., Rotor/rotor aerodynamic interactions-a Garteur action group, in: ICAS 2022, 2022, pp. 3261–3276.

[25] L. Lefevre, J. Delva, V. Nowinski, Experimental evaluation of the aerodynamic rotor/propeller interactions in hybrid compound helicopters, in: 47th European Rotorcraft Forum, 2021.

[26] R. Boisard, Numerical analysis of rotor/propeller aerodynamic interactions on a high-speed compound helicopter, J. Am. Helicopter Soc. 67 (1) (2022) 1–15, https://doi.org/10.4050/jahs.67.012005.

[27] M. Tugnoli, D. Montagnani, M. Syal, G. Droandi, A. Zanotti, Mid-fidelity approach to aerodynamic simulations of unconventional VTOL aircraft configurations, Aerosp. Sci. Technol. 115 (2021) 106804, https://doi.org/10.1016/j.ast.2021.106804.

[28] A. Zanotti, Experimental study of the aerodynamic interaction between side-by-side propellers in eVTOL airplane mode through stereoscopic particle image velocimetry, Aerospace 8 (9) (2021) 239, https://doi.org/10.3390/aerospace8090239.

[29] A. Zanotti, D. Algarotti, Aerodynamic interaction between tandem overlapping propellers in eVTOL airplane mode flight condition, Aerosp. Sci. Technol. 124 (2022) 107518, https://doi.org/10.1016/j.ast.2022.107518.

[30] H.H. Heyson, Rapid Estimation of Wind-Tunnel Corrections with Application to Wind-Tunnel and Model Design, National Aeronautics and Space Administration, 1971.
[31] Politecnico di Milano, DUST - flexible solution for aerodynamic problems, https://www.dust.polimi.it/, 2024.
[32] L. Battisti, L. Zanne, M.R. Castelli, A. Bianchini, A. Brighenti, A generalized method to extend airfoil polars over the full range of angles of attack, Renew. Energy 155 (2020) 862–875, https://doi.org/10.1016/j.renene.2020.03.150.
[33] A. Savino, A. Cocco, A. Zanotti, M. Tugnoli, P. Masarati, V. Muscarello, Coupling mid-fidelity aerodynamics and multibody dynamics for the aeroelastic analysis of rotary-wing vehicles, Energies 14 (21) (2021) 6979, https://doi.org/10.3390/en14216979.
[34] A. Cocco, A. Colli, A. Savino, P. Masarati, A. Zanotti, A non-linear unsteady vortex lattice method for aeroelastic rotor loads evaluation, in: 48th European Rotorcraft Forum (ERF 2022), 2022, pp. 1–8.